Mon. Not. R. Astron. Soc. **397,** 1153–1168 (2009) doi:10.1111/j.1365-2966.2009.14831.x

Activation of the Blandford–Znajek mechanism in collapsing stars

Serguei S. Komissarov[1⋆] and Maxim V. Barkov[1,2⋆]

[1]*Department of Applied Mathematics, The University of Leeds, Leeds LS2 9GT*
[2]*Space Research Institute, 84/32 Profsoyuznaya Street, Moscow 117997, Russia*

Accepted 2009 March 25. Received 2009 March 25; in original form 2009 February 17

ABSTRACT

The collapse of massive stars may result in the formation of accreting black holes in their interiors. The accreting stellar matter may advect substantial magnetic flux on to the black hole and promote the release of its rotational energy via magnetic stresses (the Blandford–Znajek mechanism). In this paper we explore whether this process can explain the stellar explosions and relativistic jets associated with long gamma-ray bursts. In particular, we show that the Blandford–Znajek mechanism is activated when the rest mass–energy density of matter drops below the energy density of the magnetic field in the near vicinity of the black hole (within its ergosphere). We also discuss whether such a strong magnetic field is in conflict with the rapid rotation of the stellar core required in the collapsar model, and suggest that the conflict can be avoided if the progenitor star is a component of a close binary. In this case the stellar rotation can be sustained via spin-orbital interaction. In an alternative scenario the magnetic field is generated in the accretion disc, but in this case the magnetic flux through the black hole ergosphere is not expected to be sufficiently high to explain the energetics of hypernovae by the BZ mechanism alone. However, this energy deficit can be recovered via the additional power provided by the disc.

Key words: black hole physics – MHD – relativity – methods: numerical – supernovae: general – gamma-rays: bursts.

1 INTRODUCTION

The most popular model for the central engines of long gamma-ray-burst (GRB) jets is based on the 'failed supernova' scenario of stellar collapse, or 'collapsar', where the iron core of the progenitor star forms a black hole (BH) (Woosley 1993). If the specific angular momentum in the equatorial part of the progenitor exceeds that of the marginally bound orbit of the BH, then the collapse becomes highly anisotropic. While in the polar region it may proceed more or less uninhibited, at least for a while, the equatorial layers form a dense and massive accretion disc. The gravitational energy released in this disc can be very large, more than sufficient to overturn the collapse of the outer layers and drive GRB outflows (MacFadyen & Woosley 1999). A similar configuration can be produced via in-spiralling of a BH or a neutron star into the companion star during the common envelope phase of a close binary (Tutukov & Iungelson 1979; Frayer & Woosley 1998; Zhang & Fryer 2001). In any case, the observed duration of long GRBs, between 2 and 1000 s, imposes a strong constraint on the size of progenitors – their light-crossing time should be significantly shorter than the burst duration. This implies that the progenitors must be compact stars stripped of their hydrogen envelopes. This conclusion agrees with the absence of hydrogen lines in the spectra of supernovae identified with GRBs. (Moreover, since some of these supernovae are of Type Ic their progenitors may have lost their helium envelopes as well.) Massive solitary stars can lose their envelopes via strong stellar winds. However, this may lead to unacceptably low rotation rates by the time of stellar collapse (Heger, Woosley & Spruit 2005). In the case of a binary system the loss of the envelope can be caused by gravitational interaction with the companion.

Currently, the most popular mechanism of powering GRB jets is heating via the annihilation of neutrinos and anti-neutrinos produced in the disc (MacFadyen & Woosley 1999). The energy deposited in this way is a strong function of the mass accretion rate, which must be above $\simeq 0.05\,\mathrm{M}_\odot\,\mathrm{s}^{-1}$ in order to agree with the observational constraints on the energetics of GRBs (Popham, Woosley & Fryer 1999). Such high accretion rates can be provided in the collapsar scenario, and the numerical simulations by MacFadyen & Woosley (1999) and Aloy et al. (2000) have demonstrated that sufficiently large energy deposition in the polar region above the disc may indeed result in fast collimated jets. However, we have to wait for simulations with the proper implementation of neutrino transport before making a final conclusion on the suitability of this model – the long and complicated history of numerical studies of neutrino-driven supernova explosions teaches us to be cautious. The first attempt to include neutrino transport in collapsar simulations was

⋆E-mail: serguei@maths.leeds.ac.uk (SSK); bmv@maths.leeds.ac.uk (MVB)

made by Nagataki et al. (2007), and they did not see neutrino-driven polar jets – the heating due to neutrino annihilation could not overcome the cooling due to neutrino emission.[1] In any case, it is unlikely that this model can explain bursts that are longer than 100 s, as by this time the mass accretion rate is expected to drop significantly. For example, the accretion rate in the simulations by MacFadyen & Woosley (1999) has already drifted below the critical $\dot{M} \simeq 0.05\,\mathrm{M}_\odot\,\mathrm{s}^{-1}$ by $t = 20$ s.

The two alternatives to the neutrino mechanism, which are also frequently mentioned in connection with GRBs, are magnetic braking of the accretion disc (Blandford & Payne 1982; Narayan, Paczyński & Piran 1992; Mészáros & Rees 1997; Proga et al. 2003; Uzdensky & MacFadyen 2006) and magnetic braking of the central black hole (Blandford & Znajek 1977; Mészáros & Rees 1997; Lee, Brown & Wijers 2000; McKinney 2006; Barkov & Komissarov 2008).

A number of groups have studied the potential of magnetic mechanisms in the collapsar scenario using Newtonian MHD codes and implementing the Paczynski–Witta potential in order to approximate the gravitational field of the central BH (Proga et al. 2003; Fujimoto et al. 2006; Nagataki et al. 2007). In this approach it is impossible to capture the Blandford–Znajek (BZ) effect, and only the magnetic braking of the accretion disc can be investigated. The general conclusion of these studies is that the accretion disc can launch magnetically driven jets provided the magnetic field in the progenitor core is sufficiently strong. This field is further amplified in the disc, partly due to simple winding of the poloidal component and partly due to the magneto-rotational instability (MRI), until the magnetic pressure becomes very large and pushes out the surface layers of the disc. In particular, Proga et al. (2003) studied the collapse of a star with a similar structure to that considered (MacFadyen & Woosley 1999) and with a purely monopole initial magnetic field of strength $B = 2 \times 10^{14}$ G at $r = 3r_\mathrm{g}$. The corresponding total magnetic flux, $\Psi_\mathrm{h} \simeq 10^{26}\,\mathrm{G\,cm}^2$, is in fact within the observational constraints on the fields of magnetic stars, including white dwarfs (Schmidt et al. 2003), Ap stars (Ferrario & Wickramasinghe 2005) and massive O stars (Donati et al. 2002). They used a realistic equation of state and included neutrino cooling but not heating. The simulations lasted up to $t \simeq 0.28$ s in physical time, during which a Poynting-dominated polar jet developed in the solution. The jet power seemed to show a strong systematic decline, from $\simeq 10^{51}$ erg s^{-1} down to $\simeq 10^{50}$ erg s^{-1} or even less, which might signal a transient phenomenon.

Sekiguchi & Shibata (2007) studied the collapse of rotating stellar cores and formation of BHs and their discs in the collapsar scenario using the full general relativistic magnetohydrodynamic (GRMHD) approximation. Their simulations show powerful explosions soon after the accretion disc is formed, and the free-falling plasma of the collapsing star begins to collide with this disc. However, they did not account for neutrino cooling and energy losses due to photodissociation of atomic nuclei, so these explosions could be similar in nature to the 'successful' prompt explosions of early supernova simulations (Bethe 1990). Mizuno et al. (2004a,b) carried out GRMHD simulations in the time-independent space–time of a central BH. Their computational domain did not capture the BH ergosphere and thus they could not study the role of the BZ effect (Komissarov 2004a, 2009). In addition, the energy gains/losses due to neutrino heating/cooling were not included and the equation of state (EOS) was a simple polytrope. The simulations run for a rather short time, $\simeq 280 r_\mathrm{g}/c$ where $r_\mathrm{g} = GM/c^2$, and jets were formed almost immediately, presumably due to the extremely strong initial magnetic field.

The original theory of the BZ mechanism was developed within the framework of magnetodynamics (the singular limit of the relativistic magnetohydrodynamic (RMHD) approximation where the inertia of plasma particles is fully ignored). Pioneering numerical studies of this mechanism have shown that it can also operate within the full RMHD approximation, at least in the regime where the energy density of matter is much smaller than that of the electromagnetic field, and that it can be captured by modern numerical techniques (Komissarov 2004b; Koide 2004; McKinney & Gammie 2004; Nagataki 2009). However, no systematic numerical study has been carried out in order to establish the exact conditions for activation of the BZ mechanism.

The first simulations demonstrating the potential of the BZ mechanism in the collapsar scenario were carried out by McKinney (2006), who also used a simple polytropic EOS and considered the purely adiabatic case, but captured the effects of the black hole ergosphere. The initial configuration included a torus with poloidal magnetic field and a free-falling stellar envelope. The results show ultrarelativistic jets with a Lorentz factor of up to 10 emerging from the black hole, indicating that the BZ effect may play a key role in the production of GRB jets. Barkov & Komissarov (2008) added a realistic EOS and included the energy losses due to neutrino emission (assuming an optically thin regime) and the photodissociation of nuclei. They also reported the development of relativistic outflows powered by the central black hole via the BZ mechanism (the magnetic braking of the accretion disc did not seem to contribute much to the jet power, however).

The black-hole-driven magnetic stellar explosions and relativistic jets observed in these exploratory computer simulations invite a deeper analysis of this model. Obviously, such an outcome cannot be a generic feature of core-collapse supernovae. Indeed, only a very small fraction of SNe Ib/Ic seem to produce GRBs (Piran 2005; Woosley & Bloom 2006). So what are the relevant conditions, and can they be reproduced as the results of stellar evolution? These are the main issues we address in this paper.

2 THE BLANDFORD–ZNAJEK MECHANISM AND GRBS

The rotational energy of a Kerr black hole is

$$E_\mathrm{rot} = M_\mathrm{h} c^2 f_1(a) \simeq 1.8 \times 10^{54} f_1(a) \left(\frac{M_\mathrm{h}}{\mathrm{M}_\odot}\right) \mathrm{erg}, \qquad (1)$$

where

$$f_1(a) = 1 - \frac{1}{2}\left[(1+\sqrt{1-a^2})^2 + a^2\right]^{1/2},$$

M_h is the BH mass and $a \in [0, 1)$ is its dimensionless rotation parameter. For $M_\mathrm{bh} = 2\,\mathrm{M}_\odot$ and $a = 0.9$ this gives the enormous value of $E_\mathrm{rot} \simeq 5 \times 10^{53}$ erg, which is about 50 times higher than the rotational energy of a millisecond pulsar and well above that needed to explain the energy of GRBs and associated hypernovae. Even for a relatively slowly rotating black hole with $a = 0.1$, this is still a respectable number, 2.3×10^{51} erg. Moreover, because in all versions of the collapsar model the black hole spin is aligned with

[1] However, they have simulated only the very initial stages of the collapsar evolution, $t < 2.2$ s, whereas the jet simulation of MacFadyen & Woosley (1999) started at $t = 7$ s when the density in the polar regions above the black hole has dropped down to 10^6 g cm^{-3}, leading to much lower cooling rates.

the spin of the accretion disc, this energy reserve is continuously replenished via accretion. Thus, as far as the availability of energy is concerned, the black hole model looks very promising indeed.

The energy release rate is usually estimated using the BZ power for the case of a force-free monopole magnetosphere:

$$\dot{E}_{\rm BZ} = \frac{1}{6c}\left(\frac{\Omega_{\rm h}\Psi_{\rm h}}{8\pi}\right)^2, \tag{2}$$

where $\Omega_{\rm h}$ is the angular velocity of the BH and $\Psi_{\rm h}$ is the magnetic flux threading one hemisphere of the BH horizon. (Here it is assumed that the angular velocity of the BH magnetosphere $\Omega = 0.5\Omega_{\rm h}$.) This formula is quite accurate, not only for the slowly rotating black holes considered in Blandford & Znajek (1977) but also for rapidly rotating BHs (Komissarov 2001). In application to the collapsar problem it gives us the following estimate:

$$\dot{E}_{\rm BZ} = 1.4\times10^{51} f_2(a)\Psi^2_{\rm h,27}\left(\frac{M_{\rm h}}{\rm M_\odot}\right)^{-2} {\rm erg\,s^{-1}}, \tag{3}$$

where

$$f_2(a) = a^2(1+\sqrt{1-a^2})^{-2}$$

and $\Psi_{\rm h,27} = \Psi_{\rm h}/10^{27}\,{\rm G\,cm^2}$. One can see that the power of the BZ mechanism is rather sensitive to the black hole mass and magnetic flux. Since the black hole mass is likely to be $\geq 3\,{\rm M_\odot}$, the observed energetics of hypernovae and long GRBs requires $\Psi_{\rm h,27} \simeq 1$. This value is comparable with the maximal surface flux observed in magnetic stars, Ap stars, magnetic white dwarfs and magnetars (e.g. Ferrario & Wickramasinghe 2005). Thus, the magnetic field of a GRB central engine may well be the original field of the progenitor star.

The estimates (1) and (3) show that the braking of black holes alone can explain the energetics of GRBs, and this is why this mechanism is often mentioned in the literature on GRBs. However, there is another issue to take into consideration. Equation (2) is obtained in the limit where the inertia of the magnetospheric plasma and, to a large degree, its gravitational attraction towards the black hole are ignored. In contrast, the mass density of the plasma in the collapsing star may be rather high and has to be taken into account. For example, magnetohydrodynamic waves may become trapped in the accretion flow and unable to propagate outwards. In such a case, it would not be possible to extract any of the black hole rotational energy magnetically to drive the stellar explosion, irrespective of how high this energy is. Since the BZ mechanism can only operate within the black hole ergosphere (Komissarov 2004a, 2009), the magnetohydrodynamic waves must at least be able to cross the ergosphere in the outward direction for its activation. This agrees with the conclusion reached in Takahashi et al. (1990) that the Alfven surface of a steady-state ingoing wind must be located inside the ergosphere to have the outgoing direction of the total energy flux. Thus we should consider the following condition for activation of the BZ mechanism in accretion flows: the Alfven speed has to exceed the local free-fall speed at the ergosphere,

$$v_{\rm a} > v_{\rm f}.$$

In order to simplify calculations, let us apply the Newtonian expressions for both speeds. The Alfven speed is

$$v_{\rm a}^2 = \frac{B^2}{4\pi\rho},$$

where B is the magnetic field strength and ρ is the plasma mass density, whereas the free-fall speed is

$$v_{\rm f}^2 = \frac{2GM_{\rm h}}{r}.$$

At $r = 2r_{\rm g} = 2GM/c^2$ the local criticality condition reads

$$\beta_\rho = \frac{4\pi\rho c^2}{B^2} < 1. \tag{4}$$

That is, the energy density of the magnetic field has to exceed that of the plasma in the vicinity the black hole.

For spherically symmetric flows the condition $v_{\rm a} > v_{\rm f}$ can be written as a constraint on the mass accretion rate, $\dot{M}$, and the flux of the radial magnetic field, Ψ,

$$\frac{\Psi}{2\pi r\sqrt{\dot{M}v_{\rm f}(r)}} > 1.$$

Since $v_{\rm f} \propto r^{-1/2}$, this condition is bound not to be satisfied at large r, but we only need to apply it at the ergosphere. Using $r \simeq 2r_{\rm g}$ we then obtain

$$\kappa > \kappa_{\rm c}, \tag{5}$$

where

$$\kappa = \frac{\Psi_{\rm h}}{4\pi r_{\rm g}\sqrt{\dot{M}c}} \tag{6}$$

and $\kappa_{\rm c} = 1$. In fact, the critical value of κ must depend on the black hole spin and tend to infinity for small a. Newtonian analysis cannot capture this effect. The relativistic one, on the other hand, appears rather complicated (Camenzind 1989; Takahashi et al. 1990). Fortunately, nowadays this issue can be investigated via numerical simulations. Another interesting and important issue for time-dependent simulations is whether there is only one bifurcation separating solutions with switched-on and switched-off BZ mechanism or the transition is richer and allows more complicated time-dependent solutions, e.g. quasi-periodic or chaotic ones.

3 TEST SIMULATIONS

The first type of simulation presented in this paper is designed to test the validity of our arguments behind the criterion for activation of the BZ mechanism, which we derived in Section 2 using a combination of Newtonian and relativistic physics. For this purpose we consider a more-or-less spherical accretion of cold magnetized plasma with vanishing angular momentum on to a rotating black hole. In order to focus on the MHD aspects of the problem, we ignore the microphysics important in the collapsar problem and consider a plasma with a simplified polytropic EOS.

The main details of our numerical method and various test simulations are described in Komissarov (1999, 2004b, 2006). The only really new feature here is the introduction of a Harten–Lax–van Leer (HLL) solver, which is activated when our linear Riemann solver fails. This usually occurs in regions of relativistically high magnetization where the magnetic energy density exceeds that of matter by more than one order of magnitude, or in strong rarefactions. This makes the scheme a little bit more robust although we are still forced to use a 'density floor', i.e. a lower limit on the value of mass–energy density of matter.[2]

Both in the numerical scheme and throughout this section of the paper, we utilize geometric units where $G = c = M_{\rm h} = 1$. The Kerr

[2] We have found that a total switch to the HLL solver noticeably degrades the numerical solutions via increasing numerical diffusion and dissipation. This is particularly noticeable for slowly evolving flow components, like accretion discs (see also Mignone & Bodo 2006).

space–time is described using the Kerr–Schild coordinates, so the metric form reads

$$\begin{aligned} \mathrm{d}s^2 &= g_{tt}\,\mathrm{d}t^2 + 2g_{t\phi}\,\mathrm{d}t\,\mathrm{d}\phi + 2g_{tr}\,\mathrm{d}t\,\mathrm{d}r \\ &\quad + g_{\phi\phi}\,\mathrm{d}\phi^2 + 2g_{r\phi}\,\mathrm{d}\phi\,\mathrm{d}r + g_{rr}\,\mathrm{d}r^2 + g_{\theta\theta}\,\mathrm{d}\theta^2, \end{aligned} \tag{7}$$

where

$$g_{tt} = \zeta - 1, \quad g_{t\phi} = -\zeta a \sin^2\theta, \quad g_{tr} = \zeta,$$
$$g_{\phi\phi} = \Sigma \sin^2\theta / A, \quad g_{r\phi} = -a \sin^2\theta (1+\zeta),$$
$$g_{rr} = 1 + \zeta, \quad g_{\theta\theta} = A,$$

and

$$A = r^2 + a^2\cos^2\theta,$$
$$\zeta = 2r/A,$$
$$\Sigma = (r^2 + a^2)^2 - a^2\Delta\sin^2\theta,$$
$$\Delta = r^2 + a^2 - 2r.$$

3.1 Set-up

The initial solution has to describe both the flow and the magnetic field. In this case the flow is given by the steady-state solution for unmagnetized cold plasma (dust). At infinity it is spherically symmetric and has vanishing specific angular momentum and radial velocity. The components of the four-velocity of this flow in the coordinate basis of Kerr–Schild coordinates, $\{\partial_\nu\}$, are

$$\begin{aligned} u^t &= 1 + \zeta\eta/(1+\eta), \\ u^\phi &= -a/(A(1+\eta)), \\ u^r &= -\zeta\eta, \\ u^\theta &= 0, \end{aligned} \tag{8}$$

where $\eta = \sqrt{(r^2 + a^2)/2r}$ and its rest mass density is

$$\rho = \rho_+ \left(\frac{r_+}{r}\right) \frac{1}{\eta}, \tag{9}$$

where ρ_+ is the rest mass density at the outer event horizon radius (see Appendix A).

The initial magnetic field is radial with monopole topology:

$$\begin{aligned} B^\phi &= aB^r(A + 2r)/[A\Delta + 2r(r^2 + a^2)], \\ B^r &= B_0 \sin\theta/\sqrt{\gamma}, \\ B^\theta &= 0. \end{aligned} \tag{10}$$

The azimuthal component is introduced in order to ensure that the electromagnetic fluxes of energy and angular momentum vanish (see Appendix B) and thus the initial magnetic configuration is more or less dynamically passive.

The two-dimensional axisymmetric computational domain is $(r_0 < r < r_1) \times (0 < \theta < \pi)$, where $r_0 = 1 + 0.5\sqrt{1 - a^2}$ and $r_1 = 500$. Notice that the inner boundary is inside of the outer event horizon, $r_+ = 1 + \sqrt{1 - a^2}$. This can be done because of the non-singular nature of the horizon in Kerr–Schild coordinates. The computational grid is uniform in θ, where it has 100 cells, and almost uniform in $\log r$, where it has 170 cells. The metric cell sizes are the same in both directions. The grid is divided into rings such that for any ring the metric size of its outer cells is twice that of its inner cells. The solution on each ring is advanced with its own time-step, the outer ring time-step being twice that of the inner ring. At the interface separating cells of different rings the conservation of mass, energy, momentum and magnetic flux is ensured via a simple averaging procedure.

At the inner boundary, $r = r_0$, we impose 'non-reflective' free-flow boundary conditions. The use of these conditions is justified by the fact that this boundary lies inside the outer event horizon in the region where all physical waves move inwards. At the outer boundary, $r = r_1$, we fix the flow parameters corresponding to the initial solution. In all runs the simulations are terminated well before any strong perturbation generated near the centre reaches this boundary. At the polar axis, $\theta = 0, \pi$, the boundary conditions are dictated by axial symmetry. Namely, quantities that do not vanish on the axis are reflected without change of sign, whereas quantities that vanish on the axis are reflected with change of sign.

We consider models that differ only by the rotation rate of the black hole, a, and the mass accretion rate, $\dot{M}$. For each value of a, we first deal with the model with $\kappa \simeq 1$. Depending on whether the BZ mechanism is activated in this model or not, we either increase or reduce ρ_+ (and hence $\dot{M}$) by a factor of three and compute another model. We proceed in this fashion until the solution becomes qualitatively different. Then we compute one more model based on the mean value of ρ_+ for the previous two models. After that we select the closest two models with qualitatively different solutions and show them on the bifurcation diagram summarizing the results of our study.

3.2 Results

The simulations do confirm the anticipated bifurcation and show that for a wide range of parameter a the critical value of κ is indeed close to unity. For example, the model with $a = 0.9$ and $\kappa = 1.2$ is qualitatively different from the model with $a = 0.9$ and $\kappa = 1.6$. The first model quickly settles to a steady-state accretion solution (see the top panels of Figs 1 and 2). In fact, on large scales, this solution is almost indistinguishable from the initial solution. On small scales, near the event horizon, the differences become more pronounced. In particular, a stationary accretion shock appears just outside the ergosphere. It is responsible for the jump in the rest mass density and the kinks in the magnetic field lines seen in the top left panel of Fig. 2. Inside the ergosphere the magnetization parameter μ is larger than unity, but only just. The magnetic field lines show no rotation and thus the BZ mechanism remains completely switched off.

In contrast, the model with $a = 0.9$ and $\kappa = 1.6$ exhibits powerful bipolar outflow, which drives a blast wave into the accreting flow (see the middle panel of Fig. 1). This blast wave overturns the accretion in both the polar and the equatorial directions. The black hole develops a highly rarefied magnetosphere (see the middle panels of Fig. 2), which rotates with about half of the black hole angular velocity. The shocked plasma of the accretion flow is prevented from accretion on to the black hole – instead it participates in large-scale circulations above and below the equatorial plane. The unphysical monopole configuration of the magnetic field set for this model prevents any escape of magnetic flux from the black hole. This ensures the operation of the BZ mechanism even if the confining accreting envelope is fully dispersed into the surrounding space.

For a more realistic dipolar configuration, one would expect at least partial escape of magnetic flux once the outflow is developed, and thus less power in the outflow. However, this is unlikely to affect the value of κ_c. Indeed, consider the case with a monopole field where the BZ mechanism remains switched off. Then change the polarity of the magnetic field lines in the northern hemisphere. Because the speeds of MHD waves and magnetic stresses remain invariant under the change of magnetic polarity, this will have

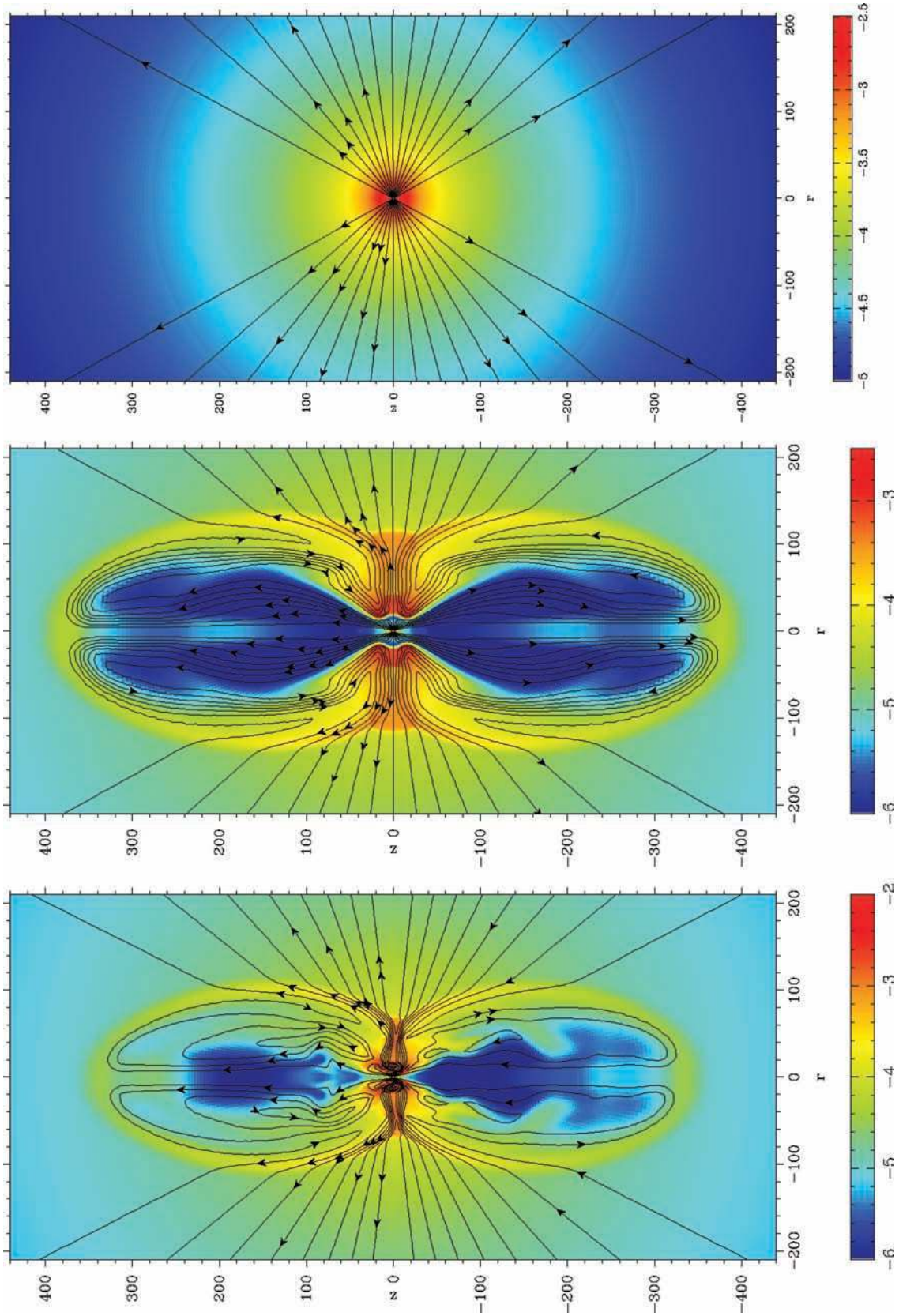

Figure 1. Free-fall accretion of a cold plasma with zero angular momentum on to a Kerr black hole ($a = 0.9$): the global structure. The colour images show $\log_{10} \rho$ in dimensionless units and the contours show the magnetic field lines. (To be more specific, the contours show the levels of poloidal magnetic flux function, Ψ. At any point (r, θ), this function gives the magnetic flux through the axisymmetric loop of radius r passing through this point.) Top panel: model with activation parameter $\kappa = 1.2$ at time $t = 2000 r_g/c$. Middle panel: model with $\kappa = 1.6$ and monopole magnetic field at time $t = 1000 r_g/c$. Bottom panel: model with $\kappa = 1.6$ and split-monopole magnetic field at time $t = 1600 r_g/c$. The unit of length is r_g.

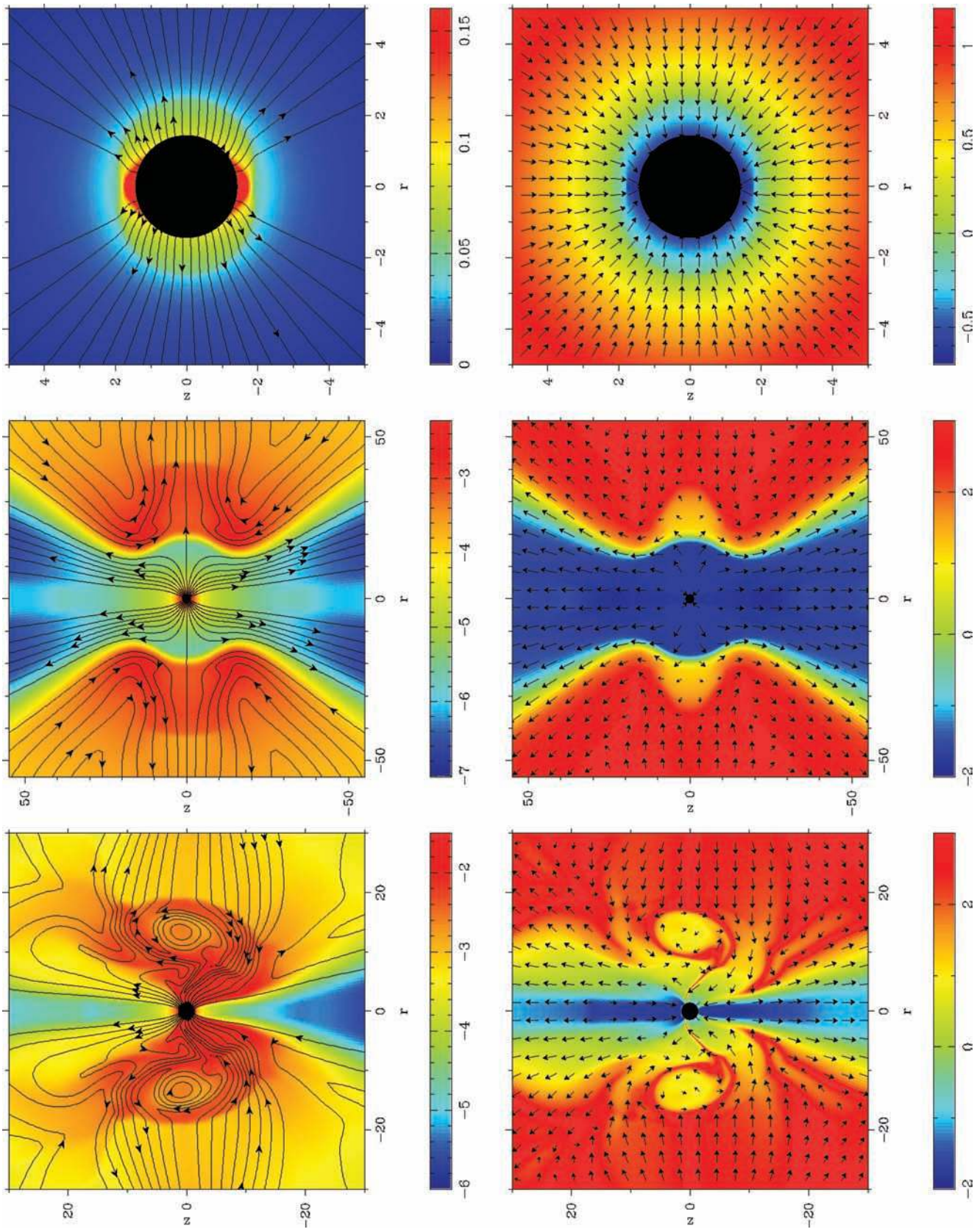

Figure 2. Free-fall accretion of a cold plasma with zero angular momentum on to a Kerr black hole ($a = 0.9$): the central regions. The top panels show the model with $\kappa = 1.2$ at $t = 2000 r_g/c$, the middle panels show the model with $\kappa = 1.6$ and monopole magnetic field at $t = 1000 r_g/c$, while the bottom panels show the model with $\kappa = 1.6$ and split-monopole magnetic field at $t = 1600 r_g/c$. The left panels show the rest mass density distribution (ρ for the top panel and $\log_{10} \rho$ for others) and the magnetic field lines. The right panels show the ratio of the proper rest mass and magnetic energy densities, $\log_{10} \beta_\rho$, and the velocity field (the length of the velocity arrow is proportional to the square root of speed).

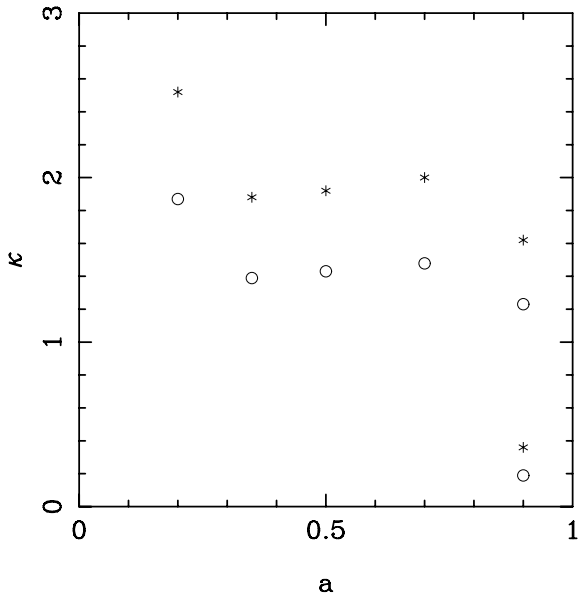

Figure 3. The bifurcation diagram. The stars show the models with the lowest value of κ that still show activation of the BZ mechanism. The circles show models with the highest value of κ for which the BZ mechanism remains turned off. The pair of points with $a = 0.9$ in the right-hand bottom corner of the diagram correspond to proper collapsar simulations. The other points show the results for test simulations.

no effect on the flow. For the very same reason, we expect activation of the BZ mechanism for exactly the same value of κ in both magnetic configurations. In order to verify this conclusion, we computed models with an initial magnetic field of split-monopole topology and the results fully agree with the expectations – the critical value of κ remains unaffected but the power of the BZ mechanism is reduced due to the partial escape of magnetic flux from the black hole. The bottom panel of Fig. 1 shows the large-scale flow developed in the model with $a = 0.9, \kappa = 1.6$ and a split-monopole initial magnetic field. The flow pattern is very similar to that of the model with a monopole field, but the expansion rate is noticeably lower, approximately by a factor of 1.8 in the polar direction and even more in the equatorial direction. The bottom panels of Fig. 2 show the inner region of this model. One can see that the accretion is no longer fully halted – the accreting plasma finds its way into the black hole in the equatorial zone and the black hole magnetosphere is confined only to the polar region of the funnel shape.

The results for $a = 0.9$ show that not only is there a bifurcation between the regimes with switched-on and switched-off BZ process, but also the critical value of the control parameter κ, and hence β_ρ, is indeed close to unity, at least for rapidly rotating black holes. The results of our parametric study, summarized in Fig. 3, show that in fact $\kappa_c(a)$ is a relatively weak function of a. It is confined within the range (1, 2) for $0.2 < a < 1.0$.

4 COLLAPSAR SIMULATIONS

The test simulations described in Section 3 allow us to determine the basic criteria for activation of the BZ mechanism in principle. However, their set-up is rather artificial, as in many astrophysical applications the accreting plasma has sufficient angular momentum to ensure the formation of an accretion disc and thus to render the approximation of spherical accretion unsuitable. This anisotropy of mass inflow is likely to make the integral activation condition (5) less helpful. On the other hand, one would expect the local condition (4) to be more-or-less robust. In order to check this, we analysed the results obtained in our current numerical study of the magnetic collapsar model.

4.1 Computational grid and boundary conditions

As in the test simulations, we use the Kerr metric in Kerr–Schild coordinates $\{\phi, r, \theta\}$. We selected $M_h = 3\ M_\odot$ and the rather optimistic value of $a = 0.9$ for the central black hole. The two-dimensional axisymmetric computational domain is $(r_0 < r < r_1) \times (0 < \theta < \pi)$, with $r_0 = (1 + 0.5\sqrt{1 - a^2})\ r_g = 5.4$ km and $r_1 = 5700 r_g = 25\,000$ km. The computational grid is of the same type as in the test simulations (Section 3.1) but with more cells, 450×180. The boundary conditions are also the same as in the test simulations.

4.2 Microphysics

For these simulations we use a realistic equation of state (EOS) that takes into account the contributions from radiation, lepton gas including pair plasma and non-degenerate nuclei (hydrogen, helium and oxygen). This is achieved via incorporation of the EOS code HELM (Timmes & Swesty 2000), which can be downloaded from the web site http://www.cococubed.com/code_pages/eos.shtml.

The neutrino cooling is computed assuming the optically thin regime and takes into account Urca processes (Ivanova, Imshennik & Nadezhin 1969), pair annihilation, photoproduction and plasma emission (Schinder et al. 1987), as well as synchrotron neutrino emission (Bezchastnov et al. 1997). In fact, Urca processes strongly dominate over other mechanisms in this problem. The photodisintegration of nuclei is included via modification of the EOS following the prescription given in Ardeljan, Bisnovatyi-Kogan & Moiseenko (2005). The equation for the mass fraction of free nucleons is adopted from Woosley & Baron (1992). We have not included the radiative heating due to annihilation of neutrinos and antineutrinos produced in the accretion disc, mainly because this requires elaborate and time-consuming calculations of neutrino transport.

4.3 Model of a collapsing star

The collapsing star is introduced using the simple free-fall model by Bethe (1990). In this model it is assumed that immediately before the collapse the mass distribution in the star satisfies the law $\rho r^3 =$ constant and that the infall proceeds with the free-fall speed in the gravitational field of the central black hole. This gives us the following radial velocity:

$$v_{\rm ff}^r = (2GM/r)^{1/2}, \tag{11}$$

and mass density

$$\rho = C_1 \times 10^7 \left(\frac{t_s}{1\,{\rm s}}\right)^{-1} \left(\frac{r}{10^7\,{\rm cm}}\right)^{-3/2} {\rm g\ cm^{-3}} \tag{12}$$

for the collapsing star, where C_1 is a constant that depends on the star mass (Bethe 1990) and t_s is the time since the start of collapse. The corresponding accretion rate and ram pressure are

$$\dot{M} = 0.056\, C_1 \left(\frac{M}{3\,M_\odot}\right)^{1/2} \left(\frac{t_s}{1\,{\rm s}}\right)^{-1} M_\odot\ {\rm s^{-1}}, \tag{13}$$

$$p_{\rm ram} = 7.9\times10^{26} C_1 \frac{M}{3\,{\rm M}_\odot}\left(\frac{t_{\rm s}}{1\,{\rm s}}\right)^{-1}\left(\frac{r}{10^7\,{\rm cm}}\right)^{-5/2}\frac{\rm g}{\rm cm\,s^2}, \quad (14)$$

respectively. For a core of radius $r_{\rm c} = 10^9$ cm and mass $3.0\,{\rm M}_\odot$ the collapse duration can be estimated as $t_{\rm c} = 2r_{\rm c}/3v_{\rm ff} \simeq 0.6$ s. Since in this study we explore the possibility of early explosion, which is soon after the core collapse, we set $t_{\rm s} = 1$ s. Because GRBs are currently associated with more massive progenitors we consider $C_1 = 3, 9$. This gives us accretion rates of $\dot{M} \simeq 0.166\,{\rm M}_\odot\,{\rm s}^{-1}$ and $\dot{M} \simeq 0.5\,{\rm M}_\odot\,{\rm s}^{-1}$ respectively.

On top of this we endow the free-falling plasma with angular momentum and a poloidal magnetic field. The angular momentum distribution is

$$l = \sin\theta \begin{cases} l_0(r\sin\theta/r_l)^2 & \text{if } r\sin\theta < r_l, \\ l_0 & \text{if } r\sin\theta > r_l, \end{cases} \quad (15)$$

where $r_l = 6300$ km and $l_0 = 10^{17}\,{\rm cm}^2\,{\rm s}^{-1}$.[3]

4.4 Initial magnetic field

The origin of the magnetic field is probably the most important and difficult issue for the magnetic model of GRBs. One possibility is that this field already exists in the progenitor and during the collapse it is simply advected on to the black hole. The recent numerical studies indicate that the poloidal and azimuthal components of the progenitor field should have similar strengths (Braithwaite & Spruit 2004). The magnetic-flux-freezing argument then suggests that during the collapse the poloidal field becomes dominant and thus in our simulations we may ignore the initial azimuthal field. As to the initial poloidal component, we adopt the solution for a uniformly magnetized sphere in vacuum.[4] To be more specific, we assume that inside the sphere of radius $r_{\rm m} = 4500$ km the magnetic field is uniform and has a strength of either $B_0 = 3\times10^9, 10^{10}$ or 3×10^{10} G, whereas outside it is described by the solution for a magnetic dipole. The selected values for the field strength allow us to capture the BZ bifurcation. Given the limitations of axisymmetry, we can only consider the case of aligned magnetic and rotational axes.

4.5 Results

Table 1 describes the key parameters of the six models investigated in this study and also summarizes the outcome of the simulations. One of the parameters, $\Psi^{\rm max}$, is the total magnetic flux enclosed by the equator of the uniformly magnetized sphere in the initial solution. Obviously, this gives us the highest magnetic flux that can be accumulated by the black hole in the simulations. Whether this maximum value is actually reached at some point depends on the progenitor rotation. For slow rotation the whole of the uniform magnetized core can be swallowed by the hole before the development of an accretion disc. At this point $\Psi_{\rm h}$ equals $\Psi^{\rm max}$, and then it begins to decline as the result of advection of the oppositely directed parts of dipolar loops (later, these loops can be clearly seen in Fig. 5).

[3] The intention was to set up a solid-body rotation within the cylindrical radius r_l; however by mistake an additional factor, $\sin\theta$, was introduced in the start-up models (the same mistake was made in the simulations described in Barkov & Komissarov (2008)). Although somewhat embarrassing, this does not affect the main results of this study.

[4] Thus, we ignore the magnetic field that is already threading the black hole by the start of the simulations.

Table 1. Summary of numerical models in collapsar simulations. $B_{0,10}$ is the initial magnetic field strength in units of 10^{10} G, C_1 is the density parameter in equation (12), $\Psi_{27}^{\rm max}$ is the maximum value of magnetic flux that can be accumulated by the black hole in units of $10^{27}\,{\rm G\,cm}^2$, $\kappa_{\rm max}$ is the value of κ corresponding to $\Psi_{27}^{\rm max}$, 'Exp' is the explosion indicator, $\Psi_{\rm h,27}$ is the actual magnetic flux accumulated by the black hole by the time of explosion, and $\dot{E}_{51}$ is the mean power of the BZ mechanism in units of $10^{51}\,{\rm erg\,s}^{-1}$.

Name	$B_{0,10}$	C_1	$\Psi_{27}^{\rm max}$	$\kappa_{\rm max}$	Exp	$\Psi_{\rm h,27}$	$\dot{E}_{51}$
A	3	3	19.1	1.07	Yes	11.6	9.6
B	3	9	19.1	0.62	Yes	13.1	12.7
C	1	3	6.67	0.36	Yes	2.80	0.4
D	1	9	6.67	0.21	No		
E	0.3	3	1.91	0.11	No		
F	0.3	9	1.91	0.06	No		

For fast rotation the accretion disc forms before $\Psi_{\rm h}$ reaches $\Psi^{\rm max}$ and after this point the growth of $\Psi_{\rm h}$ slows down noticeably, as the disc accretion is much slower compared with the free-fall accretion. Once the oppositely directed parts of the magnetic loops begin to cross the accretion shock and enter the turbulent domain that surrounds the disc, the annihilation of the poloidal magnetic field in this domain becomes an important factor. As a result, the maximum value of magnetic flux available in the solution begins to decrease before $\Psi_{\rm h}$ reaches $\Psi^{\rm max}$.

$\kappa_{\rm max}$ is the value of parameter κ computed using $\Psi^{\rm max}$ instead of the actual value of black hole flux in equation (5). A quick inspection shows that the critical value of κ based on the values of $\kappa_{\rm max}$ is about $\kappa_{\rm c} = 0.3$ (see models C and D in Table 1), almost five time lower than that in the test simulations of spherical collapse. In fact, the actual value of magnetic flux accumulated by the black hole, $\Pi_{\rm h}$, by the time of explosion is always noticeably lower than $\kappa_{\rm max}$ (see Table 1). In model C it is 2.4 times lower, thus driving the actual critical value of κ down to a value around 0.1. This result is undoubtedly connected to the highly anisotropic nature of the flow in the close vicinity of the black hole that develops in the simulations. Most importantly, there is a clear separation of the mass and magnetic fluxes: while a large fraction of mass is accreted through the accretion disc, the bulk of the magnetic field lines connected to the black hole occupy the space above (and below) the disc (see Fig. 4).

All models considered in this study first pass through the passive phase of almost spherical accretion. During this phase the black hole accumulates magnetic flux, but as $\Psi^{\rm max}$ is not sufficiently high the BZ mechanism remains switched off. Then, as the angular momentum of the plasma approaching the black hole exceeds that of the marginally bound orbit, the accretion disc forms in the equatorial plane and an accretion shock separates from its surface. This shock is best seen in the density plot of Fig. 4, where it appears as a sharp circular boundary between the light blue and dark blue areas of radius $\simeq 30r_{\rm g} \simeq 135$ km. In fact, the accretion shock oscillates in a manner reminiscent of the oscillations found earlier in supernova simulations (e.g. Blondin, Mezzacappa & DeMarino 2003; Buras et al. 2006; Scheck et al. 2008), as well as in simulations of accretion flows on to black holes (Nagakura & Yamada 2009) and attributed to the so-called stationary accretion shock instability (SASI). Most likely, the physical origin of shock oscillations in our simulations is the same, but we have not explored this issue in detail.

During this second phase, the differential rotation results in winding up of the magnetic field in the disc and its corona where the azimuthal component of the magnetic field begins to dominate

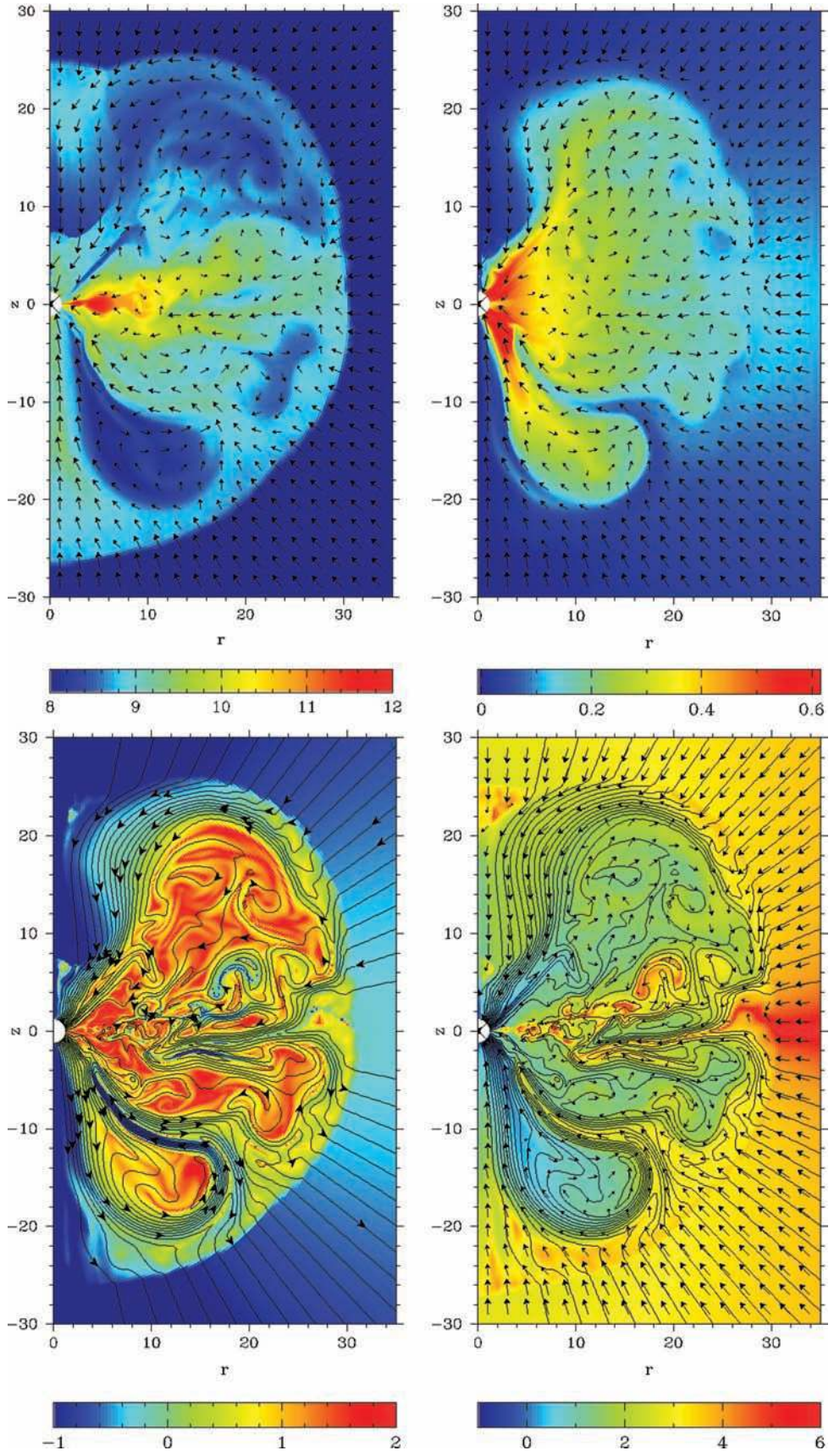

Figure 4. Model B close to the explosion, at $t = 237$ ms. Top left: $\log_{10} \rho$ and poloidal velocity; top right: angular velocity of the plasma and poloidal velocity; bottom left: ratio of azimuthal and poloidal components of the magnetic field, $\log_{10}(|\boldsymbol{B}_\phi|/|\boldsymbol{B}_\mathrm{p}|)$, and the magnetic field lines; bottom right: $\log_{10} \beta_\rho$, the magnetic field lines and the poloidal velocity field. The length of the velocity arrows is proportional to the square root of speed.

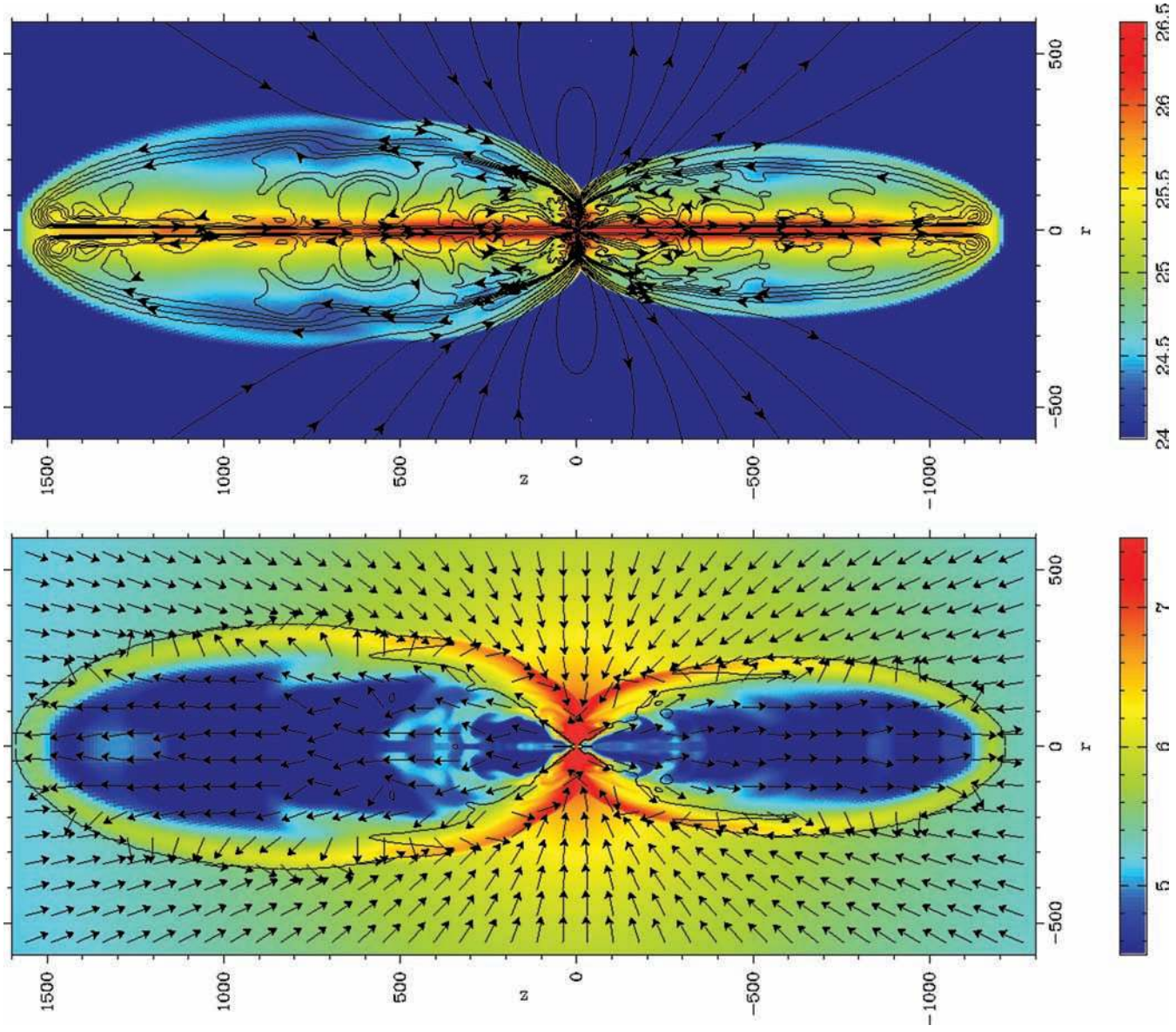

Figure 5. Model B soon after the explosion ($t = 332$ ms). Top panel: the colour image shows the total pressure, $\log_{10} p_{\rm tot}$, and the contours show the magnetic field lines. Bottom panel: the colour image gives the baryonic mass density, $\log_{10} \rho$, the arrows show the direction of flow and the contour shows the boundary separating gravitationally bounded and unbounded matter (i.e. the location where $u_{\rm t} = -1$).

(top right and bottom left panels of Fig. 4). The corona acts as a 'magnetic shield', deflecting the plasma approaching at intermediate polar angles towards either the equatorial plane or the polar axis (see Fig. 4). In models D, E and F the second phase continues until the end of the run and the BZ process remains switched off permanently. There are no clear indications suggesting that this phase may end soon, although the accretion disc grows monotonically in radius and this may eventually bring about a bifurcation.

In models A, B and C, after several oscillations the solution enters the third phase; this is characterized by a non-stop expansion of the accretion shock which then turns into a blast wave. During this transition, the black hole develops a low-mass density magnetosphere which occupies the axial funnel through which the rotational energy of the black hole is transported away away in the form of Poynting flux and powers the blast wave. The typical large-scale structure of the solution during the third phase is shown in Fig. 5 (see also Barkov & Komissarov 2008). It is rather similar to the structure observed in the simulations of spherical accretion in the case of a split-monopole magnetic field (see Section 3.2). In contrast to supersonic fluid jets, the blast wave propagates faster in the axial direction, not because of the high jet ram pressure but due to the enhancement of the thermodynamic and magnetic pressure on the jet axis associated with the z-pinch (top panel of Fig. 5). The off-axial pressure inside the cavity inflated by the jet is also quite high, and it drives the sideways expansion of the cavity and the blast wave. As one can see in the bottom panel of Fig. 5, the blast wave accelerates stellar material to speeds exceeding the local escape speed ($-u_{\rm t} > 1$) along the leading two-thirds of its length ($z > 500 r_{\rm g}$), and only near the equatorial plane does the downstream region of the shock exhibit accretion. This suggests that the black hole may not only provide ultrarelativistic GRB jets but also drive stellar explosion. Longer simulation runs are required to test this suggestion. The axisymmetry of our simulations most certainly enhances the anisotropy of the cavity expansion. Three-dimensional flow will

be subjected to kink instability, resulting in less pronounced axial compression and perhaps a more rounded blast wave, thus further increasing the chances of a proper supernova explosion.

Fig. 4 shows the solution for model B at time $t = 237$ ms, which is close to the end of the second phase, and helps us to understand how exactly the BZ mechanism is activated in our simulations. At this stage, the accretion disc is well developed and accounts for $\simeq$50–60 per cent of the mass flux through the event horizon, whereas most of the magnetic field lines threading the horizon avoid both the disc and corona that surrounds the disc and contain predominantly azimuthal magnetic fields. The strong turbulent motion in the disc and its corona must be the reason for this expulsion of magnetic flux (Zel'dovich 1957; Rädler 1968; Tao, Proctor & Weiss 1998). In any case, the observed separation of magnetic and mass fluxes results in a rather inhomogeneous magnetization of plasma near the black hole. Most importantly, there are regions that have much higher local magnetization compared with the case of spherical accretion with the same value of integral control parameter κ.

Moreover, the magnetic shield action of the disc corona can promote a further local increase of magnetization. Indeed, the corona can deflect plasma passing through the accretion shock at intermediate latitudes in a direction that does not necessarily coincide with the local direction of the magnetic field. For example, in Fig. 4 the stagnation point of post-shock flow in the upper hemisphere is located at $(r, z) \simeq (25, 20)r_{\rm g}$, whereas the separation between the magnetic field lines connected to the hole and to the disc occurs at a much lower latitude, around $(r, z) = (28, 10)r_{\rm g}$. Thus, direct mass loading of the field lines entering the shock between these points is currently suspended. On the other hand, at the other end of these field lines, where they penetrate the event horizon, their unloading continues as usual. As a result, the magnetization along these lines increases, allowing them to reach the local criticality condition, $\beta_\rho < 1$ (see the intense blue regions in the left panel of Fig. 4). Once this condition is satisfied the BZ mechanism turns on, at this point only very locally, and the initial rotation rate of the field lines is significantly lower than $0.5\Omega_{\rm h}$. However, additional magnetic energy is now being pumped into the shield via the BZ mechanism, promoting its expansion and increasing its efficiency as a flow deflector. This causes further increase of the magnetization at its base, further increase of the rotation rate of the magnetosphere and thus higher BZ power and so on. The process develops in a runaway fashion.

Fig. 6 shows the magnetization parameter β_ρ at $r = 2r_{\rm g}$ as a function of the polar angle for model B (at the same time as in Fig. 4) and for model D at a similar time. One can see that for model D the magnetization is lower. In fact, the local criticality condition, $\beta_\rho < 1$, is not satisfied anywhere for this model and this explains why an explosion is not produced in this model.[5]

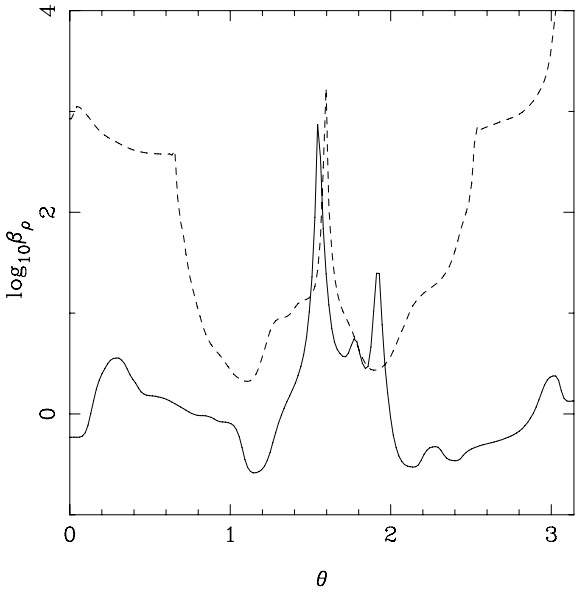

Figure 6. The magnetization parameter $\beta_\rho = 4\pi\rho\, c^2/B^2$ at $r = 2r_{\rm g}$ for models B at $t = 237$ms (solid line) and D at $t = 360$ ms (dashed line).

5 DISCUSSION

5.1 The strength and origin of the magnetic field

There seems to be only two possible origins for the magnetic field in the collapsar problem. Either it is a fossil field of the progenitor star or the field generated in the accretion disc and its corona. Here we consider both possibilities.

The blunt application of the integral condition (5) for activation of the BZ mechanism gives us the critical value of magnetic flux accumulated by the black hole,

$$\Psi_{\rm h,c} = 4.3 \times 10^{28} \left(\frac{M_{\rm h}}{3\,{\rm M}_\odot}\right) \left(\frac{\dot{M}\,{\rm s}}{{\rm M}_\odot}\right)^{1/2} {\rm G\,cm^2}.$$

Although the strength of the magnetic field in the interiors of massive stars that end up as failed supernovae is not known, this is uncomfortably high compared with the fluxes deduced from observations of 'magnetic stars', and raises doubts about the fossil hypothesis. However, the actual values of the critical magnetic flux found in our simulations are significantly lower. As we have already commented in Section 4, this is due to the anisotropy of accretion in the collapsar model. This anisotropy is expected to increase with time, as more distant parts of the progenitor with higher angular momentum enter the accretion shock (we could not study this late phase of the collapse, $t \gg 1$ s, because of various technical issues). Due to the higher angular momentum, the predominant motion downstream of the shock will be towards the equator and this should result in (i) further reduction of the mass flux and the ram pressure of accreting plasma in the polar region and (ii) more effective mass unloading of magnetic field lines entering the black hole (see Section 4.5). Both effects promote higher plasma magnetization in the polar region around the black hole, which may eventually exceed the local criticality condition (4) even in models with $\Psi_{\rm h} < 10^{27}\,{\rm G\,cm^2}$, making the fossil hypothesis more plausible.

Our results seem at odds with the Newtonian simulations by Proga et al. (2003), who obtain magnetically driven explosions powered by the disc wind within 300 ms in physical time elapsed since the start of simulations for a model with a similar mass accretion rate, $\dot{M} \simeq 0.29\,{\rm M}_\odot\,{\rm s}^{-1}$, but much lower magnetic field, $\Psi \simeq 10^{26}\,{\rm G\,cm^2}$. Since their initial model is similar to that of MacFadyen & Woosley (1999), the difference cannot be attributed to the development of the highly rarefied polar channel seen in the simulations of MacFadyen & Woosley (1999), as this only occurs several seconds later. Other possible reasons include differences in the framework, details of

[5] These results also suggest that both numerical diffusion and resistivity reduce the chances of a successful explosion in computer simulations, by smoothing the distributions of mass and magnetic field and thus decreasing the inhomogeneity of β_ρ.

the initial solutions, resolution, implementation of microphysics,[6] etc. Hopefully, simulations by other groups will soon clarify this issue.

Another factor that is likely to reduce the constraint on the strength of the fossil field, and one that is completely ignored in our simulations, is plasma heating due to neutrino–antineutrino annihilation. In the most extreme scenario, this heating completely overpowers accretion in the polar direction and drives a relativistic GRB jet (MacFadyen & Woosley 1999). Although this is an attractive model of GRB explosions by itself, we also note that the creation of a low-density funnel in this model helps to activate the BZ mechanism along the magnetic field lines that are advected inside this funnel. Thus, the neutrino heating and BZ mechanism may work hand in hand in driving GRBs and hypernovae.

Even in failed supernovae, the stellar core collapse does not lead directly to the formation of a black hole but the progenitor still proceeds through the proto-neutron star (PNS) phase first. If the period of the PNS is very short, around several milliseconds, its rotational energy is sufficient to modify strongly the direction of collapse and the initial conditions for the black hole phase. In particular, magnetic stresses due to either fossil or MRI-generated magnetic fields can drive powerful bipolar outflows (Moiseenko, Bisnovatyi-Kogan & Ardeljan 2006; Obergaulinger et al. 2006; Burrows et al. 2007). As reported by Burrows et al. (2007), these outflows can coexist with equatorial accretion and may not be able to prevent the eventual collapse of a PNS. However, they certainly overcome accretion in the polar direction and create favourable conditions for activation of the BZ mechanism. The very fast rotation of the progenitor Fe core required in this scenario, with a period around a few seconds, is unlikely to be achieved in stars with strong fossil magnetic field (see Section 5.2).

A related issue is whether a significant fraction of the magnetic flux available in the progenitor can actually be accumulated by the black hole. The traditional viewpoint is that the inward advection of the magnetic field in the accretion disc is effective and can result in the build-up of poloidal magnetic field up to equipartition with the disc gas pressure (Bisnovatyi-Kogan & Ruzmaikin 1974, 1976; Blandford & Znajek 1977; Macdonald & Thorne 1982; Begelman, Blandford & Rees 1984). On the other hand, it has also been argued that in a standard viscosity-driven accretion disc the turbulent outward diffusion of poloidal field may easily neutralize the inward advection well before it reaches equipartition strength (Lubow, Papaloizou & Pringle 1994; Heyvaerts, Priest & Bardou 1996; Ghosh & Abramowicz 1997; Livio, Ogilvie & Pringle 1999). However, the disc angular momentum can also be removed by magnetic stresses via interaction with the disc corona and wind, and this may change the balance in favour of the inward accretion of poloidal magnetic flux (Spruit & Uzdensky 2005; Robstein & Lovelace 2008). This has been demonstrated in recent three-dimensional Newtonian simulations of radiatively inefficient accretion discs, where the poloidal magnetic field reached equipartition strength near the central 'black hole' (Igumenshchev 2008). In our simulations, a significant fraction of the magnetic flux of the black hole is accumulated before the development of the accretion disc. However, the flux does not escape after the disc is formed. On the contrary, it keeps increasing until the oppositely directed magnetic field lines begin to enter the accretion shock. Thus, our results are in agreement with those by Igumenshchev (2008) and suggest strong magnetic interaction between the disc and its corona/wind.

An alternative origin of the magnetic field is via dynamo processes in the turbulent accretion disc. In this case the saturated equilibrium magnetic field strength can be estimated from the energy equipartition argument:

$$\frac{B_{\rm t}^2}{8\pi} \simeq \rho \frac{v_{\rm t}^2}{2}, \tag{16}$$

where $B_{\rm t}$ and $v_{\rm t}$ are the turbulent magnetic field and velocity respectively. However, the typical scale of this field is rather small, of the order of the disc height, $h \ll r_{\rm g}$. When magnetic loops of such small scale are advected on to the black hole, one would expect quick, on the time-scale of $r_{\rm g}/c$, reconnection and annihilation of the magnetic field, resulting in low residual magnetic flux penetrating the black hole. Tout & Pringle (1996) argued that similar reconnection processes in the disc corona may lead to an inverse cascade of magnetic energy on scales exceeding h. The expected spectrum in this range is $B_\lambda \propto 1/\lambda$, and thus on the scale of $r_{\rm g}$ one could find a regular magnetic field of strength

$$B_{\rm p} \simeq \frac{h}{r_{\rm g}} B_{\rm t}.$$

The standard theory of α discs gives

$$v_{\rm t} \simeq \alpha \Omega_k h,$$

where Ω_k is the Keplerian frequency, h is the half-thickness of the disc and $\alpha = 0.1$–0.01 is a free parameter of this theory. According to the theory of thin neutrino-cooled accretion discs by Popham et al. (1999),

$$\frac{h}{r} = 0.09 \left(\frac{\alpha}{0.1}\right)^{0.1} \left(\frac{M_{\rm h}}{{\rm M}_\odot}\right)^{-0.1} \left(\frac{r}{r_{\rm g}}\right)^{0.35}$$

and

$$\rho = 2.4 \times 10^{15} \left(\frac{\alpha}{0.1}\right)^{-1.3} \left(\frac{M_{\rm h}}{{\rm M}_\odot}\right)^{-1.7} \left(\frac{r}{r_{\rm g}}\right)^{-2.55} \left(\frac{\dot{M}\,{\rm s}}{{\rm M}_\odot}\right) \frac{\rm g}{{\rm cm}^3}.$$

Putting all these equations together, we find the typical black hole magnetic flux

$$\Psi_{\rm h} = 3 \times 10^{26} \left(\frac{\alpha}{0.1}\right)^{0.55} \left(\frac{M_{\rm h}}{{\rm M}_\odot}\right)^{0.95} \left(\frac{\dot{M}\,{\rm s}}{{\rm M}_\odot}\right)^{0.5} {\rm G\,cm^2}. \tag{17}$$

The corresponding power of the BZ mechanism is

$$\dot{E}_{\rm BZ} \simeq 1.3 \times 10^{50} f_2(a) \left(\frac{\alpha}{0.1}\right)^{1.1} \left(\frac{\dot{M}\,{\rm s}}{{\rm M}_\odot}\right) {\rm erg\,s^{-1}}, \tag{18}$$

almost independently of the black hole mass. One can see that even for maximally rotating black holes one should not expect much more than 10^{51} erg from the collapse of a $10\,{\rm M}_\odot$ progenitor. On the other hand, in this model one should expect a much more powerful magnetically driven wind from the accretion disc (Livio et al. 1999). Mass loading of this wind is likely to be much higher due to processes similar to solar coronal mass injections, and the terminal Lorentz factors are not expected to be as high as required from the GRB observations. However, the disc wind could be responsible for the $\sim 10^{52}$ erg required to drive hypernovae. Having said that, we need to warn the reader that the above equations are purely Newtonian and thus their application to the near vicinity of a black hole may introduce large errors. Moreover, the current theory of magnetic dynamos in accretion discs can hardly be called well-developed, and so one might expect a few surprises as our understanding of the dynamo improves. Finally, the above picture

[6] In particular, Proga et al. (2003) state that neutrino cooling is dominated by pair annihilation, whereas we find that it is the lepton capture of free nucleons that is dominant in our models.

is in conflict with our numerical models, particularly those that do not show BZ-driven explosions. It is difficult to pin down the exact reasons for this, but the key issues are likely to be the condition of axisymmetry and the numerical resolution.

5.2 The nature of the rotation

With a typical rotation rate of $200\,\mathrm{km\,s^{-1}}$ on the zero-age main-sequence (e.g. Penny 1996; Howarth et al. 1997), the standard evolutionary models of solitary stars predict very rapid rotation of stellar cores by the time of collapse (Heger, Langer & Woosley 2000; Hirschi, Meynet & Maeder 2004, 2005). According to these models, the typical periods of newly born pulsars in successful supernovae are around one millisecond and 'failed supernovae' conceive rapidly rotating black holes with accretion discs, as required for GRBs. These results, however, contradict the observations, which clearly indicate that young millisecond pulsars and GRBs are much more rare.

When the magnetic torque due to the relatively weak magnetic field generated via the Tayler–Spruit dynamo (Tayler 1973; Spruit 2002) is included in the evolutionary models, they result in significant spin-down of stellar cores during the red giant phase and during the intensive mass-loss period characteristic for massive stars at the Wolf–Rayet phase (Heger et al. 2005). As a result, the predicted rotation rates for newly born pulsars come into agreement with the observations but, on the other hand, the core rotation becomes too low compared with that required for the collapsar model of GRBs (Heger et al. 2005). Recently, it was proposed that low metallicity could be the factor that allows us to reduce the efficiency of magnetic braking in GRB progenitors (Yoon & Langer 2005; Woosley & Heger 2006; Yoon et al. 2006). On one hand, the mass-loss rate decreases significantly with metallicity, leading to a significant reduction in loss of angular momentum. On the other hand, low-metallicity stars rotating at around 50 per cent of the break-up speed may become chemically homogeneous due to rotationally induced mixing. As a result they avoid the development of extended envelopes and slowing down of the stellar cores via interaction with such envelopes. However, the magnetic field of magnetic stars is much stronger than predicted by the Tayler–Spruit theory of stellar dynamos, and thus magnetic braking progenitors are more severe in our magnetic model of a GRB central engine that relies on a strong fossil magnetic field.[7]

The above complication seems to be specific to solitary stars and can be avoided in close binaries. First, the extended envelope of a giant star is only weakly bounded by gravity and is easily dispersed in a close binary, predominantly in the orbital plane (Taam & Sandquist 2000). Secondly, even in the case of high metallicity and/or strong magnetic field, the stellar rotation rate may remain high due to the synchronization of spin and orbital motions. Indeed, the minimum separation between the components of the binary star, L_c, is determined by the size of the critical Roche surfaces, as

$$L_\mathrm{c} \simeq 2.64 R q^{0.2}, \tag{19}$$

where R is the radius of the more massive component and q is the ratio of the component masses ($q \leq 1$). The rotational period is given by

$$\Omega^2 = (1+q)\frac{GM}{L^3}, \tag{20}$$

where L is the actual separation of the component and M is the mass of the more massive component. Using $q = 1, L = 3R, R = 5\,\mathrm{R}_\odot$ and $M = 20\,\mathrm{M}_\odot$, we find that the specific angular momentum on the stellar equator is about $6 \times 10^{18}\,\mathrm{cm^2\,s^{-1}}$. On the other hand, the specific angular momentum of the marginally bound orbit around the Schwarzschild black hole is

$$l_\mathrm{mb} = 4\frac{GM_\mathrm{h}}{c}. \tag{21}$$

For $M_\mathrm{h} = 20\,\mathrm{M}_\odot$, this gives us only $3.5 \times 10^{17}\,\mathrm{cm^2\,s^{-1}}$. Thus, when the star collapses one would expect the black hole to develop substantial rotation and to become surrounded by an accretion disc towards the final phase of the collapse (Barkov & Komissarov 2008, in preparation). The lower accretion rates expected in this phase make the neutrino mechanism much less effective, but do not have much of an effect on the BZ mechanism. Indeed, assuming the equipartition of gas and magnetic pressure, we find that

$$B^2 = 8\pi p = 8\pi\alpha^{-2}\rho v_\mathrm{t}^2.$$

Applying this at the inner edge ($r = r_\mathrm{g}$) of a neutrino-cooled accretion disc (Popham et al. 1999), we can estimate the maximum magnetic flux that can be kept at the black hole by the disc advection as

$$\Psi_\mathrm{h} = 3.3 \times 10^{28}\left(\frac{\alpha}{0.1}\right)^{-0.55}\left(\frac{M_\mathrm{h}}{\mathrm{M}_\odot}\right)^{1.05}\left(\frac{\dot{M}\,\mathrm{s}}{\mathrm{M}_\odot}\right)^{0.5}\mathrm{G\,cm^2}. \tag{22}$$

For $M_\mathrm{h} = 20\,\mathrm{M}_\odot$ and $\mathrm{M}_\odot = 0.01\,\mathrm{M}_\odot\,\mathrm{s}^{-1}$ this gives us the formidable $\Psi_\mathrm{h} \simeq 7 \times 10^{28}\,\mathrm{G\,cm^2}$. According to equation (3), much lower fluxes are needed to explain the observed energetics of GRBs.

Even faster rotation is expected in the case of the merger of a helium star with its compact companion, a neutron star or a black hole, during the common envelope phase of a close binary (Tutukov & Iungelson 1979; Frayer & Woosley 1998; Zhang & Fryer 2001). Since the orbital angular momentum of the binary star is

$$J_\mathrm{orb}^2(L) = \frac{GM_\mathrm{h}^2M^2L}{M_\mathrm{h}+M}, \tag{23}$$

where M_h is the mass of the compact star, we can roughly estimate the specific orbital angular momentum deposited at distance r from the centre of the helium star as

$$l^2(r) = J_\mathrm{orb}^2(r)/M^2(r) = \frac{GM_\mathrm{h}^2 r}{M_\mathrm{h}+M(r)}, \tag{24}$$

where $M(r)$ is the helium star mass within radius r. When $M(r)$ is a slow function, as it is in Bethe's model where $M(r) \propto \ln r$, we may use in equation (24) the total mass of the helium star, M, in place of $M(r)$. For $M_\mathrm{bh} = 2\,\mathrm{M}_\odot$ and $M_\mathrm{hc} = 20\,\mathrm{M}_\odot$ this gives us

$$l(r_9) = 1.5 \times 10^{17}\sqrt{r_9}\ \mathrm{cm^2\,s^{-1}}, \tag{25}$$

where $r_9 = r/10^9$ cm. In spite of all the approximations, such estimates agree quite well with the results of numerical simulations (Zhang & Fryer 2001). For $r_9 > 1$ this is higher than the upper value of $l = 10^{17}\,\mathrm{cm^2\,s^{-1}}$ imposed in the collapsar simulations by MacFadyen & Woosley (1999). The higher angular momentum is one of the factors that reduces the disc accretion rates and hence the efficiency of the neutrino annihilation mechanism (Zhang & Fryer 2001) but, as we have already commented, for the BZ mechanism this is much less of a problem.

The compact companion may initially be a neutron star, but during the in-spiral it is expected to accumulate substantial mass and become a black hole (Zhang & Fryer 2001). In fact, during the in-spiralling the compact companion accumulates not only mass but

[7] The magnetic field of magnetic stars is most likely to be inherited from the interstellar medium during star formation (Moss 1987; Braithwaite & Spruit 2004).

spin as well. The final value of the black hole rotation parameter computed in Zhang & Fryer (2001) varies from model to model between $a = 0.14$ and $a = 0.985$. Thus, provided that the normal star of the common envelope binary is a magnetic star, we have all the key ingredients for a successful magnetically driven GRB explosion: (i) a rapidly rotating black hole, (ii) a rapidly rotating and (iii) compact collapsing star, and (iv) a 'fossil' magnetic field that is strong enough to tap the black hole energy at rates required by observations (see equation 3). It has been noted many times that the magnetic fluxes of magnetic Ap stars, magnetic white dwarfs and pulsars are remarkably similar (e.g. Ferrario & Wickramasinghe 2005), suggesting that they could be related. Now one may consider adding another type of object to this list – GRB collapsars.

5.3 Connection between the stellar explosion and GRB jets

It is important to understand whether the same physical mechanism can be responsible for both the stellar explosion and GRB jets, and whether those events are simultaneous or time-separated. For example, while the BZ mechanism could energize highly collimated GRB jets, the neutrino- or magnetically-driven disc wind could energize a more isotropic supernova blast. Our simulations suggest that the BZ mechanism could be capable of simultaneously driving both the supernova blast and the GRB jets, as the explosive expulsion of stellar matter in the polar direction coexists with its accretion in the equatorial plane. However, additional simulations will be needed to see whether this duality is not temporal and can be preserved for periods comparable with the durations of long GRBs. In fact, the interplay between a 'failed' supernova and GRB jet could be rather intricate. For a start, a full-scale supernova explosion could cut off the mass supply to the black hole accretion disc and thus terminate the production of GRB jets. In this case, a long-duration GRB may still be produced later, when some of the supernova ejecta fall back to form a secondary accretion disc. On the other hand, by the time of cut-off the energy deposited in the blast may not be sufficient for a proper explosion and the mass supply is almost fully restored some time later during the early fall-back phase, leading to re-ignition of the GRB engine as well. These active periods may repeat several times during the lifetime of a collapsar. Alternatively, one can imagine a completely different scenario where the GRB jets reach the stellar surface before the supernova explosion is fully developed. Then the hot cocoon plasma quickly escapes through the opening into the surrounding space, the pressure in the cavity drops and the supernova shock dies out. It seems that only large-scale numerical simulations can clarify this issue. Yet, such a numerical study represents a major challenge as three-dimensional effects are likely to be significant if not crucial.

6 CONCLUSIONS

In this paper we continued our study into the potential of the BZ mechanism as the main driver in the central engine of gamma-ray bursts. In particular, we analysed the conditions for activation of the mechanism in the collapsar model, where accumulation of magnetic flux by the central black hole is likely to be a byproduct of stellar collapse.

It appears that the rotating black hole begins to pump energy into the surroundings, and overpowers accretion only when the rest mass energy density of matter drops below the energy density of the electromagnetic field near the ergosphere (see equation 4). Only under this condition can the MHD waves generated in the ergosphere transport energy and angular momentum away from the black hole.

In the case of spherical accretion, the above criterion can be written as a condition on the total magnetic flux accumulated by the black hole and the total mass accretion rate (see equation 5). However, in the case of non-spherical accretion, characteristic for the collapsar model, this integral condition becomes less applicable due to the spatial separation of the magnetic field and accretion flow inside the accretion shock. In fact, our numerical simulations show explosions for significantly lower magnetic fluxes compared with those expected from the integral criterion. We have not included neutrino heating in our numerical models. This is another factor that can make activation of the BZ mechanism in the collapsar set-up easier.

Both general energetic considerations and the condition for activation of the BZ mechanism require the central black hole to accumulate magnetic flux comparable to the highest observed values for magnetic stars, $\Psi \simeq 10^{27}\,\mathrm{G\,cm^2}$. Current evolutionary models of massive solitary stars indicate that a fossil field of such strength should slow down the rotation of helium cores below the rate required for the formation of accretion discs around the black holes of failed supernovae. The conflict between the strong fossil magnetic field and the rapid stellar rotation required by the BZ mechanism may be resolved in models where the GRB progenitor is a component of a close binary. In this case, the high spin of the progenitor can be sustained at the expense of the orbital rotation. Moreover, the strong gravitational interaction between the components of a close binary helps to explain the compactness of GRB progenitors deduced from the observed durations of bursts.

The magnetic field can also be generated in the accretion disc and its corona, but in this case the magnetic flux through the black hole ergosphere is not sufficiently high to explain the power of hypernovae by the BZ mechanism alone. On the other hand, in this case the disc is expected to drive a MHD wind more powerful than the BZ jet. Although such a wind is unlikely to reach the high Lorentz factors deduced from the observations of GRB jets (due to high mass loading), it could be behind the observed energetics of hypernovae.

ACKNOWLEDGMENTS

This research was funded by STFC under the rolling grant "Theoretical Astrophysics in Leeds".

REFERENCES

Aloy M. A., Muller E., Abner J. M., Marti J. M., MacFadyen A. I., 2000, ApJ, 531, L119
Ardeljan N. V., Bisnovatyi-Kogan G. S., Moiseenko S. G., 2005, MNRAS, 359, 333
Barkov M. V., Komissarov S. S., 2008, MNRAS, 385, L28
Begelman M. C., Blandford R. D., Rees M. J., 1984, Rev. Mod. Phys., 56, 255
Bethe H. A., 1990, Rev. Mod. Phys., 62, 801
Bezchastnov V. G., Haensel P., Kaminker A. D., Yakovlev D. G., 1997, A&A, 328, 409
Bisnovatyi-Kogan G. S., Ruzmaikin A. A., 1974, Ap&SS, 28, 45
Bisnovatyi-Kogan G. S., Ruzmaikin A. A., 1976, Ap&SS, 42, 401
Blandford R. D., Payne D. G., 1982, MNRAS, 199, 883
Blandford R. D., Znajek R. L., 1977, MNRAS, 179, 433
Blondin J. M., Mezzacappa A., DeMarino C., 2003, ApJ, 584, 971
Braithwaite J., Spruit H. C., 2004, Nat, 431, 819
Buras R., Janka H.-Th., Rampp M., Kifonidis K., 2006, A&A, 457, 281

Burrows A., Dessart L., Livne E., Ott C. D., Murphy J., 2007, ApJ, 664, 416
Camenzind M., 1989, in Belvedere G., ed., Accretion disks and magnetic fields in astrophysics. Kluwer, Dordrecht, p. 129
Donati J.-F., Babel J., Harries T. J., Howarth I. D., Petit P., Semel M., 2002, MNRAS, 333, 55
Ferrario L., Wickramasinghe D. T., 2005, MNRAS, 356, 615
Frayer C. L., Woosley S. E., 1998, ApJ, 502, L9
Fujimoto S., Kotake K., Yamada S., Hashimoto M., Sato K., 2006, ApJ, 644, 1040
Ghosh P., Abramowicz M. A., 1997, MNRAS, 292, 887
Heger A., Langer N., Woosley S. E., 2000, ApJ, 528, 368
Heger A., Woosley S. E., Spruit H. C., 2005, ApJ, 626, 350
Mészáros P., Rees M. J., 1997, ApJ, 482, L29
Hirschi R., Meynet G., Maeder A., 2004, A&A, 425, 649
Hirschi R., Meynet G., Maeder A., 2005, A&A, 443, 581
Heyvaerts J., Priest E. R., Bardou A., 1996, ApJ, 473, 403
Howarth I. D., Siebert K. W., Hussain G. A., Prinja R. K., 1997, MNRAS, 284, 265
Igumenshchev I. V., 2008, ApJ, 677, 317
Ivanova L. N., Imshennik V. S., Nadezhin D. K., 1969, Sci. Inf. Astron. Council Acad. Sci., 13, 3
Koide S., 2004, ApJ, 606, L45
Komissarov S. S., 1999, MNRAS, 303, 343
Komissarov S. S., 2001, MNRAS, 326, L41
Komissarov S. S., 2004a, MNRAS, 350, 427
Komissarov S. S., 2004b, MNRAS, 350, 1431
Komissarov S. S., 2006, MNRAS, 368, 993
Komissarov S. S., 2009, J. Kor. Phys. Soc., 54, 2503
Lee H. K., Brown G. E., Wijers R. A. M. J., 2000, ApJ, 536, 416
Livio M., Ogilvie G. I., Pringle J. E., 1999, ApJ, 512, 100
Lubow S. H., Papaloizou J. C. B., Pringle J. E., 1994, MNRAS, 267, 235
Macdonald D. A., Thorne K. S., 1982, MNRAS, 198, 345
MacFadyen A. I., Woosley S. E., 1999, ApJ, 524, 262
McKinney J. C., 2006, MNRAS, 368, 1561
McKinney J. C., Gammie C. F., 2004, ApJ, 611, 977
Mignone A., Bodo G., 2006, MNRAS, 368, 1040
Misner C. W., Thorne K. S., Wheeler J. A., 1973, Gravitation. W. H. Freeman and Co., San Francisco
Mizuno Y., Yamada S., Koide S., Shibata K., 2004a, ApJ, 606, 395
Mizuno Y., Yamada S., Koide S., Shibata K., 2004b, ApJ, 615, 389
Moiseenko S. G., Bisnovatyi-Kogan G. S., Ardeljan N. V., 2006, MNRAS, 370, 501
Moss D., 1987, MNRAS, 226, 297
Nagakura H., Yamada S., 2009, ApJ, 696, 2026
Nagataki S., 2009, ApJ, submitted (arXiv:0902.1908)
Nagataki S., Takahashi R., Mizuta A., Takiwaki T., 2007, ApJ, 659, 512
Narayan R., Paczyński B., Piran T., 1992, ApJ, 395, L8
Obergaulinger M., Aloy M. A., Dimmelmeier H., Muller E., 2006, A&A, 457, 209
Penny L. R., 1996, ApJ, 463, 737
Piran T., 2005, Rev. Mod. Phys., 76, 1143
Popham R., Woosley S. E., Fryer C. L., 1999, ApJ, 518, 356
Proga D., MacFadyen A. I., Armitage P. J., Begelman M. C., 2003, ApJ, 629, 397
Rädler K.-H., 1968, Z. Naturforsch. A, 23, 1851
Robstein D. M., Lovelace R. V. E., 2008, ApJ, 677, 1221
Scheck L., Janka H.-Th., Foglizzio T., Kifonidis K., 2008, A&A, 477, 931
Schinder P. J., Schramm D. N., Wiita P. J., Margolis S. H., Tubbs D. L., 1987, ApJ, 313, 531
Schmidt G. D. et al., 2003, ApJ, 595, 1101
Sekiguchi Y., Shibata M., 2007, Prog. Theor. Phys., 117, 1029
Spruit H. C., 2002, A&A, 381, 923
Spruit H. C., Uzdensky D. A., 2005, ApJ, 629, 960
Taam R. E., Sandquist E. L., 2000, ARA&A, 38, 113
Takahashi M., Niita S., Tatematsu Y., Tomimatsu A., 1990, ApJ, 363, 206
Tao L., Proctor M. R. E., Weiss N. O., 1998, MNRAS, 300, 907
Tayler R., 1973, MNRAS, 161, 365
Timmes F. X., Swesty F. D., 2000, ApJS, 126, 501
Tout C. A., Pringle J. E., 1996, MNRAS, 281, 219
Tutukov A., Iungelson L., 1979, in Mass loss and evolution of O-type stars. Reidel, Dordrecht, p. 401
Uzdensky D. A., MacFadyen A. I., 2006, ApJ, 647, 1192
Woosley S. E., 1993, ApJ, 405, 273
Woosley S. E., Baron E., 1992, ApJ, 391, 228
Woosley S. E., Bloom J. S., 2006, ARA&A, 44, 507
Woosley S. E., Heger A., 2006, ApJ, 637, 914
Yoon S.-C., Langer N., 2005, A&A, 443, 643.
Yoon S.-C., Langer N., Norman C., 2006, A&A, 460, 199
Zel'dovich Ya.B., 1957, Sov. Phys. JETP, 4, 460
Zhang W., Fryer C. L., 2001, ApJ, 550, 357

APPENDIX A: DUST ACCRETION IN KERR–SCHILD COORDINATES

The problem of dust accretion has been considered in Misner, Thorne & Wheeler (1973). In the coordinate basis of Boyer–Lindquist coordinates, $\{\partial/\partial x^{\nu'}\}$, the components of the four-velocity of a dust particle accreting from rest at infinity and having zero angular momentum are

$$\begin{aligned} u^{t'} &= 1 + \zeta(r^2 + a^2)/\Delta, \\ u^{\phi'} &= 2a\zeta/\Delta, \\ u^{r'} &= -\zeta\eta, \\ u^{\theta'} &= 0, \end{aligned} \tag{A1}$$

where $\eta = \sqrt{(r^2 + a^2)/2r}$. In order to find the four-velocity components in the coordinate basis of Kerr–Schild coordinates, one can simply use the corresponding transformation law (Komissarov 2004a):

$$\begin{aligned} \mathrm{d}t &= \mathrm{d}t' + (2r/\Delta)\,\mathrm{d}r', \\ \mathrm{d}\phi &= \mathrm{d}\phi' + (a/\Delta)\,\mathrm{d}r', \\ \mathrm{d}r &= \mathrm{d}r', \\ \mathrm{d}\theta &= \mathrm{d}\theta'. \end{aligned} \tag{A2}$$

This gives us

$$\begin{aligned} u^t &= 1 + \zeta\eta/(1 + \eta), \\ u^\phi &= -a/[A(1 + \eta)], \\ u^r &= -\zeta\eta, \\ u^\theta &= 0. \end{aligned} \tag{A3}$$

Notice that in both coordinate systems the particles move over a conical surface, $\theta = \mathrm{const}$. Their rotation about the symmetry axis is due to the inertial-frame dragging effect.

In order to find the density distribution, consider the steady-state version of the continuity equation:

$$\partial_r(\sqrt{-g}\rho u^r) = 0,$$

where $g = -\sin^2\theta A^2$ is the determinant of the metric tensor in Kerr–Schild (and Boyer–Lindquist) coordinates. This shows that

$$\sqrt{-g}\rho u^r = C(\theta),$$

where $C(\theta)$ is some arbitrary function, and then that

$$\rho(r, \theta) = \frac{C(\theta)}{\sin\theta\sqrt{2r(r^2 + a^2)}}.$$

At infinity this function does not depend on the polar angle only if $C \propto \sin\theta$, which implies that ρ does not depend on θ for any r.

Denoting the rest mass density at the outer event horizon as ρ_+, we may now write

$$\rho = \rho_+ \left(\frac{r_+}{r}\right) \frac{1}{\eta}. \tag{A4}$$

APPENDIX B: INITIAL MAGNETIC FIELD

In this section we employ the 3 + 1 splitting of electrodynamics described in Komissarov (2004a), where the electromagnetic field is represented by four three-vectors: $\boldsymbol{D}$, $\boldsymbol{E}$, $\boldsymbol{B}$ and $\boldsymbol{H}$, defined via

$$B^i = \alpha\, {}^*F^{it}, \tag{B1}$$

$$E_i = \frac{\alpha}{2} e_{ijk}\, {}^*F^{jk}, \tag{B2}$$

$$D^i = \alpha F^{ti}, \tag{B3}$$

$$H_i = \frac{\alpha}{2} e_{ijk} F^{jk}, \tag{B4}$$

where ${}^*F^{\mu\nu}$ is the Faraday tensor, $F^{\mu\nu}$ is the Maxwell tensor, e_{ijk} is the Levi–Civita tensor of space and α is the lapse function. In the stationary metric, $\partial_t g_{\nu\mu} = 0$, the evolution of these vector fields is described by the Maxwell equations for electromagnetic fields in matter. The effects of curved space–time are incorporated via the non-Euclidian spatial metric and the constitutive equations:

$$\boldsymbol{E} = \alpha \boldsymbol{D} + \boldsymbol{\beta} \times \boldsymbol{B}, \tag{B5}$$

$$\boldsymbol{H} = \alpha \boldsymbol{B} - \boldsymbol{\beta} \times \boldsymbol{D}, \tag{B6}$$

where α is the lapse function and β is the shift vector. In terms of these vectors the condition of perfect conductivity, $F_{\nu\mu}\, u^\mu = 0$, can be written in the familiar form

$$\boldsymbol{E} = -\boldsymbol{v} \times \boldsymbol{B}, \tag{B7}$$

where $v^i = \mathrm{d}x^i/\mathrm{d}t$ is the usual three-velocity vector.

Both in Boyer–Lindquist and the Kerr–Schild coordinates, the poloidal component of Poynting flux, $S^i = -\alpha\, T^i{}_{\rm t}$, is given by

$$\boldsymbol{S}_{\rm p} = \boldsymbol{E}_{\mathbf{p}} \times \boldsymbol{H}_{\boldsymbol{\phi}} + \boldsymbol{E}_{\boldsymbol{\phi}} \times \boldsymbol{H}_{\mathbf{p}}, \tag{B8}$$

whereas the the poloidal component of the angular momentum flux, $L^i = \alpha T^i{}_\phi$, is

$$\boldsymbol{L}_{\rm p} = -(\boldsymbol{E} \cdot \boldsymbol{m})\boldsymbol{D}_{\rm p} - (\boldsymbol{H} \cdot \boldsymbol{m})\boldsymbol{B}_{\rm p}, \tag{B9}$$

where $\boldsymbol{m} = \partial/\partial\phi$.

Suppose that in Boyer–Lindquist coordinates the magnetic field is purely radial, $\boldsymbol{B}'_\theta = \boldsymbol{B}'_\phi = 0$. Since $\boldsymbol{\beta} \| \boldsymbol{m}$, equation (B6) then implies that

$$\boldsymbol{H}'_\phi = \alpha \boldsymbol{B}'_\phi = 0.$$

Provided this magnetic field is frozen into the flow described by equation (A1), we also find that

$$\boldsymbol{E}' = -\boldsymbol{v}'_{\boldsymbol{\phi}} \times \boldsymbol{B}'_{\boldsymbol{r}}.$$

Given these results, the equations (B9) and (B8) ensure that

$$\boldsymbol{S}'_{\rm p} = \boldsymbol{L}'_{\rm p} = 0.$$

In order to find the corresponding electromagnetic field in the Kerr–Schild coordinates we simply apply the transformation law A2). This way we find that

$$\boldsymbol{S}_{\rm p} = \boldsymbol{L}_{\rm p} = 0 \tag{B10}$$

and

$$B^\theta = 0, \quad B^\phi = B^r \frac{a(A + 2r)}{A\Delta + 2r(r^2 + a^2)}. \tag{B11}$$

The divergence-free condition requires

$$\partial_r(\sqrt{\gamma} B^r) = 0$$

and hence

$$B^r = \frac{f(\theta)}{\sqrt{\gamma}},$$

where γ is the determinant of the spatial metric. Provided that at infinity (where $\gamma \propto \sin^2\theta$) B^r does not depend on the polar angle, we then have

$$B^r = B_0 \frac{\sin\theta}{\sqrt{\gamma}}. \tag{B12}$$

This paper has been typeset from a TEX/LATEX file prepared by the author.